Neural network modeling and analysis of the material removal process during laser machining

Evgueni Bordatchev

International Journal of Advanced Manufacturing Technology

Int J Adv Manuf Technol (2003) 22: 41–53
DOI 10.1007/s00170-002-1441-9

ORIGINAL ARTICLE

Basem F. Yousef · George K. Knopf
Evgueni V. Bordatchev · Suwas K. Nikumb

Neural network modeling and analysis of the material removal process during laser machining

Received: 11 February 2002 / Accepted: 6 June 2002 / Published online: 19 March 2003

Abstract To manufacture parts with nano- or micro-scale geometry using laser machining, it is essential to have a thorough understanding of the material removal process in order to control the system behaviour. At present, the operator must use trial-and-error methods to set the process control parameters related to the laser beam, motion system, and work piece material. In addition, dynamic characteristics of the process that cannot be controlled by the operator such as power density fluctuations, intensity distribution within the laser beam, and thermal effects can significantly influence the machining process and the quality of part geometry. This paper describes how a multi-layered neural network can be used to model the nonlinear laser micro-machining process in an effort to predict the level of pulse energy needed to create a dent or crater with the desired depth and diameter. Laser pulses of different energy levels are impinged on the surface of several test materials in order to investigate the effect of pulse energy on the resulting crater geometry and the volume of material removed. The experimentally acquired data is used to train and test the neural network's performance. The key system inputs for the process model are mean depth and mean diameter of the crater, and the system outputs are pulse energy, variance of depth and variance of diameter. This study demonstrates that the proposed neural network approach can predict the behaviour of the material removal process during laser machining to a high degree of accuracy.

Keywords Laser micro-machining · Pulse energy · Crater geometry · Artificial neural network

B.F. Yousef · G.K. Knopf
Department of Mechanical and Materials Engineering,
The University of Western Ontario, London, N6A 5B9, Canada
E-mail: gknopf@engga.uwo.ca
Tel.: +1-519-661-2111 ext. 88452
Fax: +1-519-661-3020

E.V. Bordatchev · S.K. Nikumb
Integrated Manufacturing Technologies Institute,
National Research Council of Canada, London, Canada

1 Introduction

Laser beams are used extensively for a variety of material-removal applications because they provide highly concentrated energy sources that can be easily transmitted and manipulated. Micro-mechanical structures are becoming more common with the ever increasing demand for new micro-fabrication tools. As feature sizes become smaller and smaller, i.e. typically below 100 μm, conventional mechanical approaches to cutting, drilling and shaping materials may be replaced with photon or particle beam techniques that enable geometric features as small as laser wavelengths (smaller than a micrometer) to be created with a high degree of precision and repeatability. In addition, laser fabrication processes are non-contact, dry, and clean operations that enable ease of automation.

Machining with a laser beam is a complex dynamic process with numerous parameters as shown in Fig. 1. The nonlinear behaviour of the laser-material interactions play a significant role in forming the final surface profile and the resultant geometry of the machined micro-features. The need to precisely control a large number of parameters, often with random components [1], makes the task of improving the process performance very difficult. Moreover, modeling all these factors using conventional, analytical and numerical methods poses a substantial challenge. In practice, the operator has to perform a number of experiments to set the appropriate process control parameters related to the laser apparatus, motion control system, and piece material. This trial-and-error approach is costly and time consuming especially for a small batch production or prototyping, and does not ensure near *optimality* with a given set of process conditions and manufacturing objectives.

Since the invention of lasers in 1960, many studies have been undertaken to understand, control and improve the performance of the laser material removal process. Some of the investigative studies deal with the

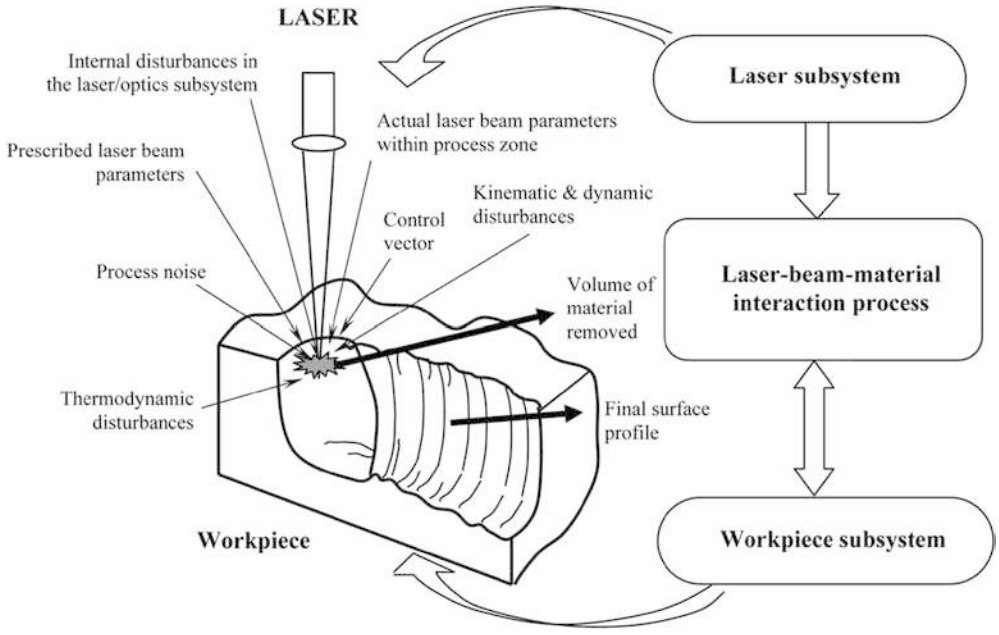

Fig. 1 Laser machining system [1] and control parameters

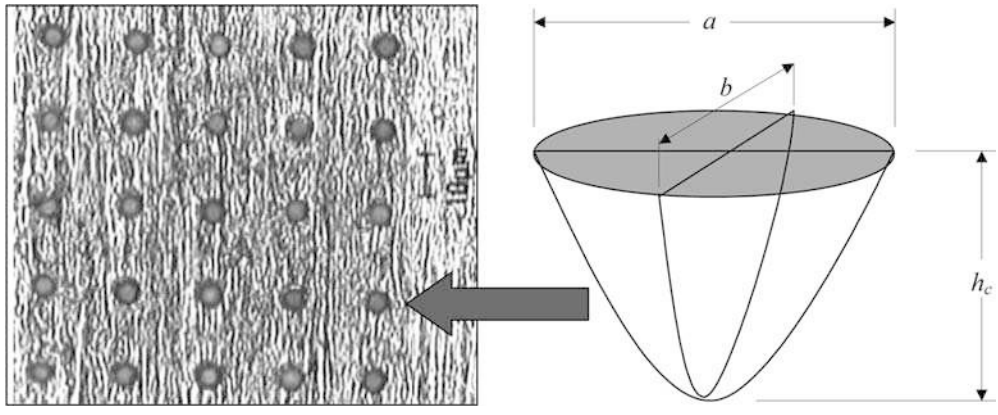

Fig. 2 The geometric parameters used to model the crater dimensions where h_c is the depth, a is the major diameter and b is the minor diameter. The average diameter for each sample, $d_c = \frac{a+b}{2}$, is computed for analysis

heat dissipation problem by considering a moving heat source on a flat surface that can be either a point source [2], a line source [3], a uniform distribution of heat in a disk shape [4], a cylindrical source [5], or a Gaussian distribution [6]. Other researchers have explored the problem of melt ejection and attempted to find a connection between the striated aspect of the kerf lateral walls and a periodic phenomenon in the cutting process such as small perturbations generating waves on the liquid metal surface [7], or forced oscillations resulting from the equation of the energy balance [8]. Another group of studies dealt with the oxygen reaction in fusion laser cutting by taking the thermodynamic approach [9], or performing chemical analysis of the ejected particles and the solidified metal in the kerf [10].

By visual means, Yoshiaki [11] tried to determine the optimum conditions of the process performance. In 1981, these researchers [12] again tried to improve the cut quality (surface roughness and out-of-flatness) through controlling the clinging dross by introducing two techniques to reduce or eliminate the dross.

Finite element modeling and analysis of the evaporating cutting process that uses a moving high energy pulsed laser with a two-dimensional unsteady heat transfer equation was introduced by Kim et al [13, 14, 15]. Numerical analysis was carried out on the amount of material removed, groove smoothness with laser power, and number of pulses, while other laser cutting parameters are fixed.

An analytical model was developed by Kaebernick et al [16] to predict the quality of the cut under various process conditions. The model was based on an infinitesimal point heat source representing the effect of the laser beam on the surfaces inside the cutting zone and included the contribution of the oxygen reaction to the heating of the metal. Other researchers utilized artificial intelligence methodology to improve laser-machining performance. Toth [17] used a self-organizing Kohonen feature map, a sub-class of artificial neural networks, as a controller for a pulsed laser surface polishing process.

Most of these research activities can be divided into two categories, i.e. theoretical and experimental

approaches. Theoretical approaches tackle the process using analytical and computational methods, which usually do not cover all the experimental aspects related to the process such as change in ambient temperature, heating of material which may lead to changes in the physical properties of the material, heat loss by conduction and convection. These approaches also represent the process under certain conditions and specific assumptions such as constant surface reflectivity of the material, that the material moves at a constant relative velocity, the material is isotropic and opaque with constant thermal and optical properties, and that the material is perfectly clean of impurities and dirt. Therefore, the expected results from such models are non-comprehensive and different from the real experimental outputs of the process. In contrast, experiment-oriented approaches give more realistic results, but involve limited operating conditions of a process under specific conditions. For instance, the experimental research of Toth [17] provided an unconventional approach that derives its functionality from the adaptive properties of the controller in a changing environment, but the results obtained using this approach could only be applied to surface polishing.

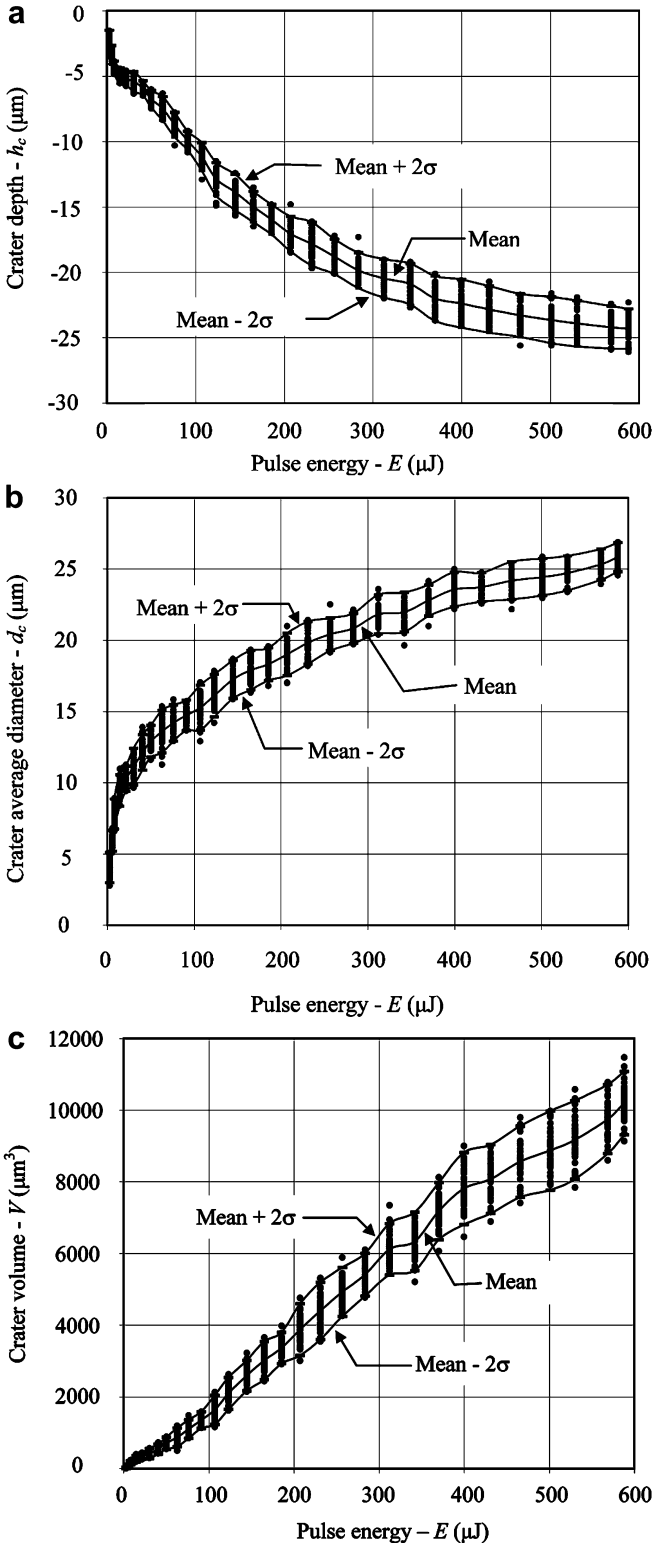

Fig. 3a–c Experimentally measured crater parameters formed on a brass specimen. **a** Crater depth as a function of pulse energy (μJ). **b** Average diameter d_c of crater as a function of pulse energy (μJ). **c** Volume of material removed as a function of pulse energy (μJ)

Since the work presented in this paper is based on the crater geometry resulting from the interaction of work piece material foil with a single laser pulse, this research provides the needed insight for improving the micromanufacturing process. Therefore the primary goal is to investigate, analyze and model how the geometry of the crater and final surface profile is formed and how they depend on the level of incident laser pulse energy. As a result, an artificial neural network model of the micromachining process has been developed in order to find more satisfactory process parameters for a particular machining set-up.

The proposed neural network model provides a powerful platform from which important process control information can be conveniently obtained and applied to the development of better prediction models for novel applications that use a variety of materials. Furthermore, the results obtained provide valuable insight into the future development of quantitative prediction capabilities in other fast advancing regimes of the field. The neural network model also enables better process design, reduces the need for trial-and-error methods, eliminates the need for frequent experimental trials, and minimizes the need for post-machining operations due to improved quality.

2 Background

Experimental information obtained from the laser micro-machining process, such as input-output data, can be used to form a model of the system. One approach to creating a non-linear functional map between measured inputs and outputs involves an artificial neural network (ANN). The strength of neural computing structures lies in their ability to learn and adapt to changing environmental conditions [18].

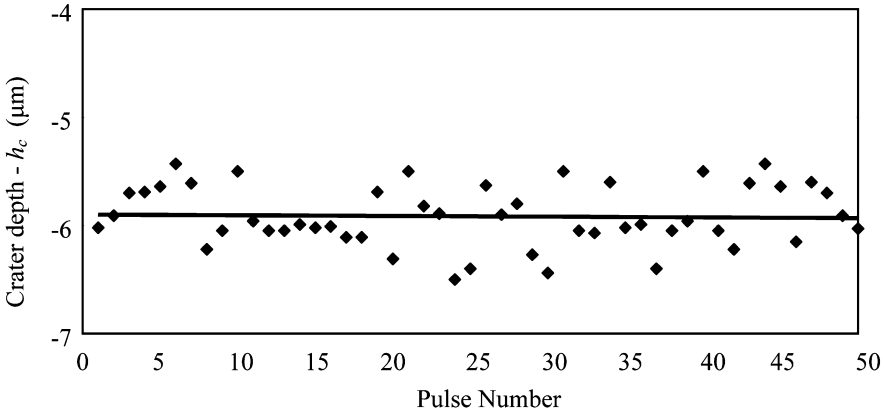

Fig. 4 Variations in the crater depth for the same amount of pulse energy

2.1 Artificial neural network

The main component of a neural network is the neuron that performs a nonlinear weighted summation of the applied inputs. The input signals x_i ($i=1,2,\ldots, p$) are applied to the network. Once received by the neuron, they are modified by the interconnection weights w_{ji}, where w_{ji} is the interconnection weight between input x_i and neuron j. All weighted inputs to a particular neuron are summed along with a bias weight w_{jo} to produce a single result u_j. Mathematically, the output of neuron j can be expressed as

$$y_j = f(\mathbf{W}(n)^{\mathrm{T}}\mathbf{X}(n)) \tag{1}$$

where y_i is the output of neuron j, $\mathbf{W}(n)$ is the interconnection weight vector, T is the transpose, $\mathbf{X}(n)$ is the input signal vector for iteration n, and $f(\cdot)$is the activation function. The nonlinear activation, or transfer, function [18] can be given by

$$f(\cdot) = \frac{1}{1+e^{-a(\cdot)}} \tag{2}$$

Individual neurons are able to perform only simple mathematical or logic operations. Complex input-output behaviour can only be modeled by connecting numerous simple neurons in multi-layered structures [18]. To model a manufacturing process such as laser micromachining, the neural network must undergo both training and operation phases. During the training phase, the neurons in the first layer of the network are fed with a randomly selected input $x_i(n)$. Each neuron j in layer l computes an output $y^l_j(n)$, based on the interconnection weight $w^l_{ji}(n)$, and transmits the response to the next layer's neurons as an input, and so on, until the signal is moved forward through the network. At the output layer, 0, the desired output d_k of neuron k is compared with the model output of the neuron $y^0{}_k(n)$. Since the outputs, in general, will not be the same as the desired values, an error signal $e_j(n)$ initiates at the output neurons and back propagates through the layers of the network updating the interconnection weights by a step change Δw^l_{ji} (n). After the network completes the feed-forward pass of the computed output signal by each neuron, and the back-propagation pass of the error signal that updates the weights, another input/output training pair is implemented to the network and the process is repeated. This weight adaptation process continues until a set of weights and biases that satisfies all input-output pairs is obtained. The algorithm for training the neural network is described in the Appendix.

2.2 Experimental data

Experiments were conducted to provide a clear picture of the physics behind the laser micro-machining process and to provide the neural network model with the necessary input-output information. Two series of tests were carried out to investigate the capabilities of the neural network. The first was to model the process when a single-material (brass) data set is involved and the second, when 3-material (brass, copper and stainless steel) data sets are involved.

In the first series of tests, a brass foil was impinged with laser pulses of different energies to investigate the effect of pulse energy on the resulting crater geometry and the volume of material removed. Using a diode pumped Nd:YAG laser, 50 craters were produced with each pulse energy. The laser machined crater matrix and the geometric parameters used to model the crater dimensions are shown in Fig. 2. Simple geometry was used to describe the crater geometry and further simplify necessary calculations such as the volume of the crater which was approximated using:

$$V = \frac{\pi}{2} abh_c \tag{3}$$

where h_c is the depth, and a and b are the diameters along two directions.

Crater depths and diameters along two profiles (a and b) were measured and the average diameter d_c was calculated for each sample. When the crater depth was plotted against the pulse energy as shown in Fig. 3a, it became clear that the laser machining process produced craters with different depths at the same level of pulse energy. The variation in depth created by the machining

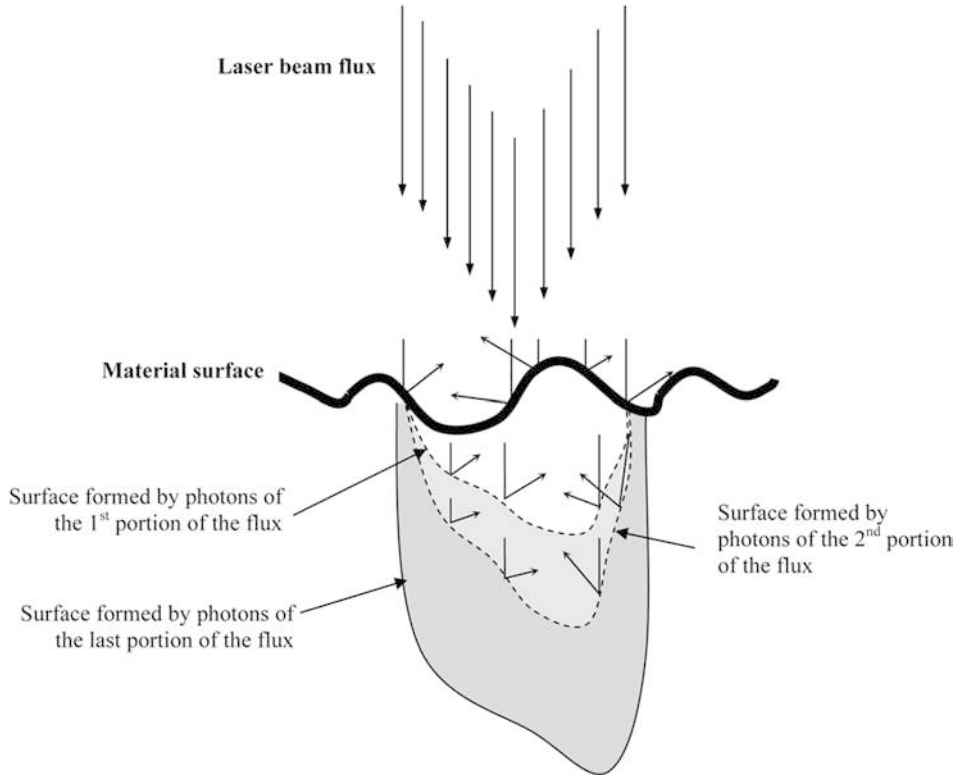

Fig. 5 Laser pulse and material interaction during crater formation

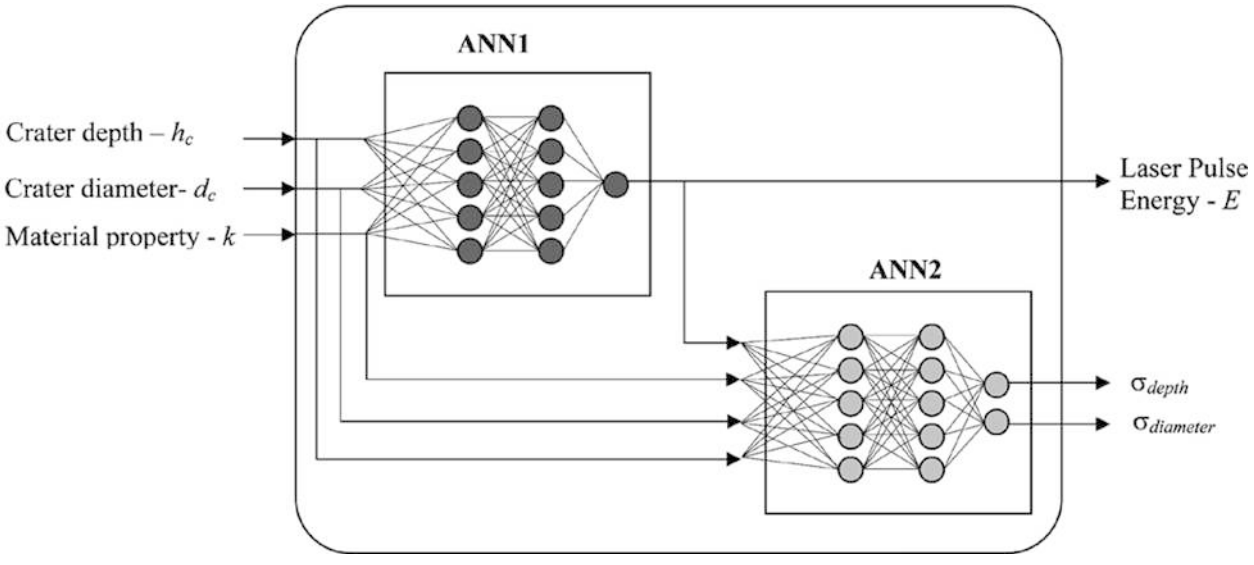

Fig. 6 The interconnection of the two neural networks used in the proposed algorithm for predicting the pulse energy (E) needed to produce the desired crater geometry (h_c, d_c). For the single-material tests, the material property input k is set to zero

process is referred to as the *haze around the mean*. Furthermore, Fig. 3a illustrates that the haze around the mean increases as the pulse energy increases. Similar variations are observed for crater diameter (Fig. 3b), and for the volume of material removed (Fig. 3c). Additionally, these figures demonstrate that the haze around the mean is less for low energy levels than higher energies because the chance for heat loss in the work piece is significantly lower. Consequently, the small haze region at low energies implies that laser machining operations performed with low pulse energy levels will do less damage to the work piece and produce a higher-quality cut.

The behaviour of the curves can be attributed to specific *process parameters*. Since cutting speed (or feed-rate), frequency, and duration of pulse are not involved in these experiments, there are two main factors that could cause this behaviour, i.e. variation within the pulse energy, and the dynamics of the laser-material interaction. The first factor provides an explanation for the

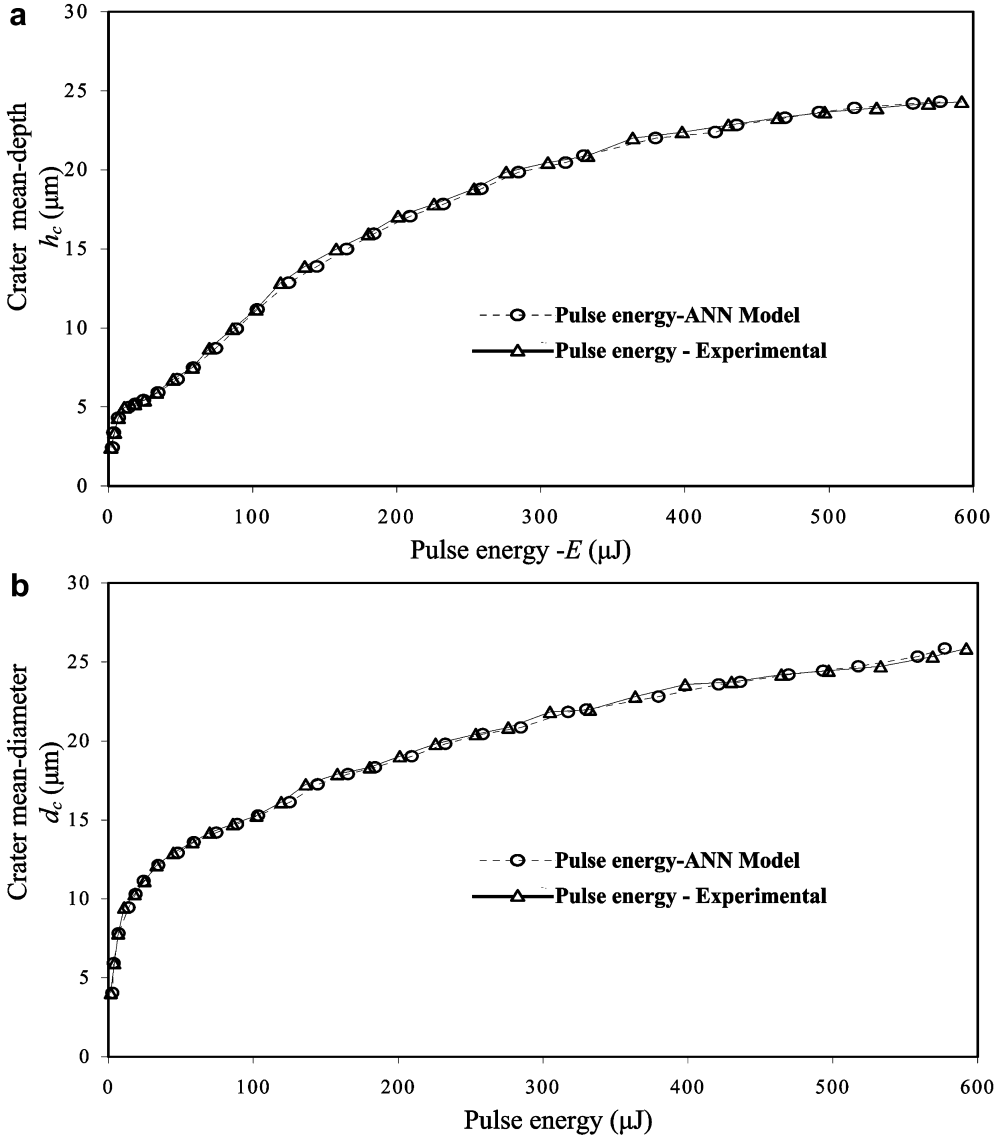

Fig. 7a–b Crater parameters corresponding to experimental and neural network predicted energy levels. **a** Mean depth of crater for experimental and ANN predicted pulse energies (brass) **b** Mean diameter of crater for experimental and ANN predicted pulse energies (brass)

haze around the mean. Theoretically, the pulse energy is assumed to be constant if the same Q-switch is used. However, this is not a valid assumption because the actual energy generated will change from one pulse to another through the same Q-switch. Figure 4 illustrates the variation in depth of material removed by pulses having a constant energy level of 40.4 μJ. The same characteristics are obtained if the diameter or the volume is plotted against pulse number.

The effect of the second factor can be explained by referring to Fig. 5. One can imagine the layer of volume removed from the material depends on several parameters including the wave front of the focused laser beam profile, beam mode characteristics, surface reflectivity of the work piece material, and its original profile which include the surface irregularities at each point of the local area struck by wave front photons. Subsequently, impingement of photons within the single pulse defines the conformed shape of the crater and so on, as shown in Fig. 5. This interaction results in an additive randomization in material removal inside the crater once the crater starts to deepen. When experiments were carried out using other materials such as stainless steel and copper, similar curve characteristics were observed.

3 Results and analysis

Two back-propagation neural networks are used to model the relationship between crater dimensions and pulse energy. Modeling the laser machining process involved the following two stages. The first stage of the artificial neural network (ANN1) is used to model the relationship between the pulse energy and the mean depth and mean diameter of the crater for a specified material. The output energy computed in the first stage, along with the desired depth h_c, and diameter d_c, are used as inputs to the second-stage network (ANN2), and the generated outputs from this network are the

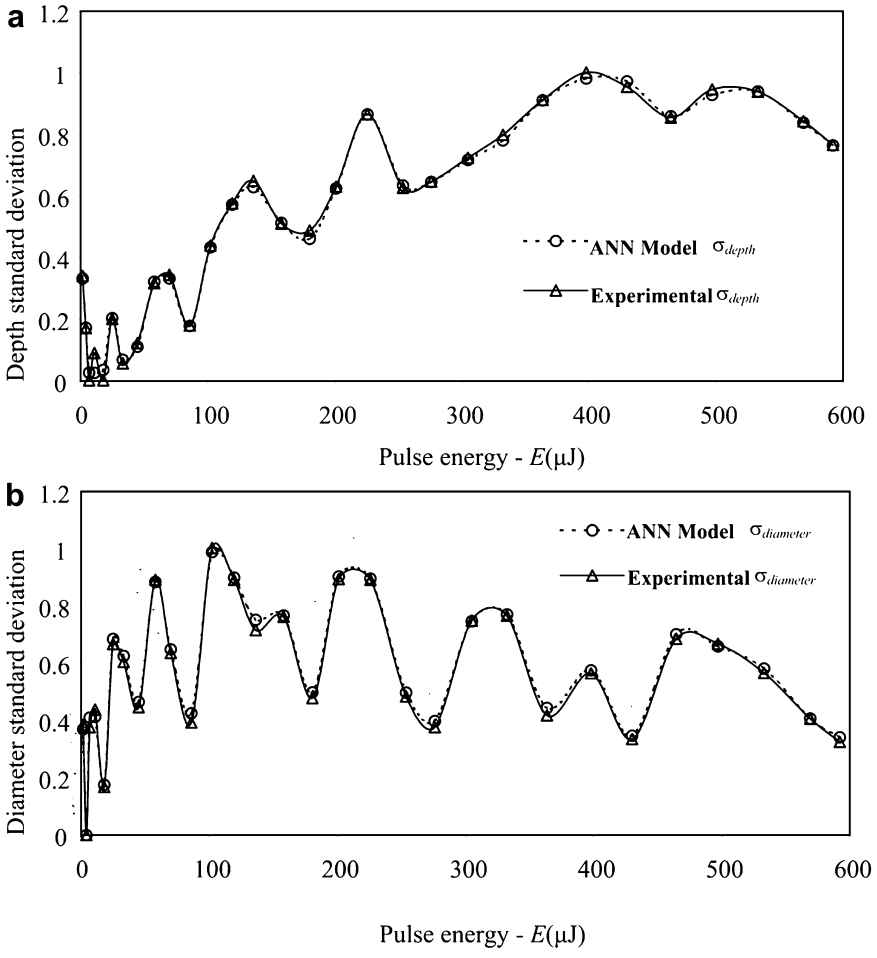

Fig. 8a–c Variations in the crater parameters for experimental and neural network predicted energy levels. **a** Standard deviation of crater depth for various levels of pulse energy **b** Standard deviation of crater diameter for various levels of pulse energy

standard deviations σ_{depth} and σ_{diameter} associated with that depth and diameter.

The two neural networks are interconnected so that ANN2 computes a certainty measure for the first network's output. For example, ANN1 predicts the level of energy E_1 needed to produce a pulse crater of depth h_c and average diameter d_c. The second network, ANN2, predicts the uncertainty associated with the crater dimensions by giving the standard deviations of depth and diameter, and these in turn give the expected variation in the produced crater depth and diameter. Figure 6 shows the control box that describes the two networks in their operation mode.

3.1 Tests using a single material

Both ANN1 and ANN2 were trained using the experimentally acquired data. The weight values of the neural networks were initially set to small random values between ± 0.1 and iteratively adjusted using the back-propagation training algorithm [18]. After each network converged to a pre-set error value between the experimental data and ANN model outputs, the final weight vectors were used to investigate the model of the laser machining process. The mean depth and mean diameters were used as test inputs. The statistical nature of the original data implies that there is not a one-to-one mapping between an input (crater dimensions) and output (pulse energy). Consequently, only the statistical mean properties could be examined and evaluated.

3.1.1 *Case 1: Specific crater depth and diameter*

The first test involved creating a map between pulse energy and the required crater depths and diameters for brass material. Experimental data and model results for the 6×6 ANN1 network are shown in Fig. 7a and b. The investigation into a single material demonstrates that the proposed neural network was able to predict the pulse energy needed to create specific crater dimensions.

3.1.2 *Case 2: Variations of crater depth and diameter*

The second test involved modeling the variations (standard deviations) in the depth and diameter associated with a specified energy level using the ANN2 network. The outputs of the 20×5 network are shown in Fig. 8a and b. Again, the figure demonstrates that ANN2 could successfully model the actual process output.

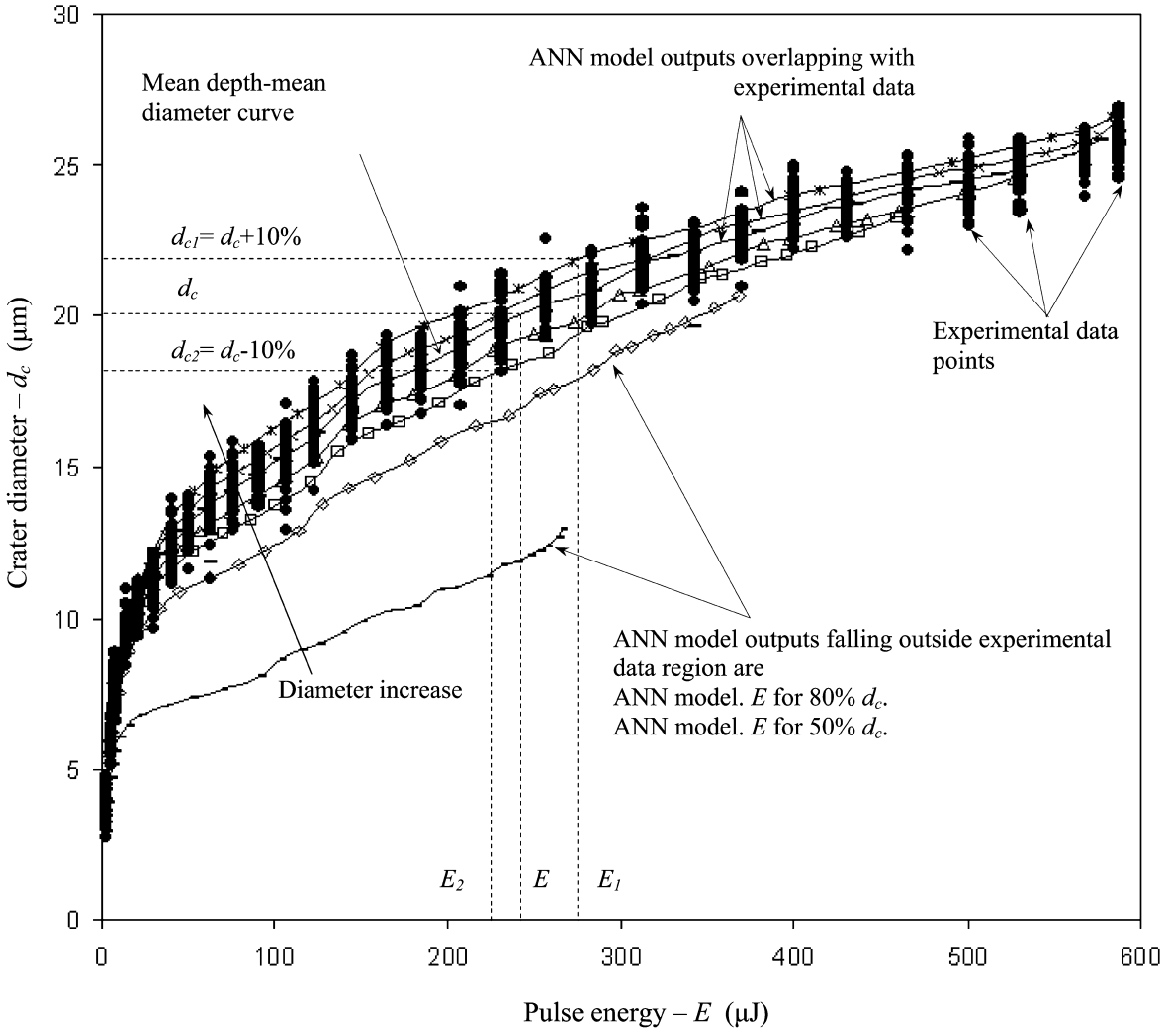

Fig. 9 Experimental data and neural network results of the laser machining process

The number of neurons in the first hidden layer and number of epochs during training play significant roles in the algorithm's performance. The number of neurons in the network is responsible for defining the main features of the anticipated output curve such as the order of the curve and the segments at which the curve changes the direction of its slope. In addition, the number of epochs during training is responsible for tuning the curve features while details which are picked up by the first layer neurons move it closer to the solution.

3.1.3 *Case 3: Effect of changing pulse energy on crater diameter*

The third series of tests were used to model the effect of changes in pulse energy on the crater diameter when using the ANN1 network. Tests were performed for the following diameter changes: 50%, 80%, 90%, 95%, 105% and 110% of mean diameter. In the first set of tests, the mean diameter and mean depth values were applied as inputs to the network and the output was the pulse energy. The tests are then repeated by increasing and decreasing the diameter by a predefined percentage so that each diameter, together with the depth that had been used in the first run, were used as inputs to the model. For instance, while the inputs of the first run were the mean depth and mean diameter, the inputs for the second run were the same mean depth (unchanged) and 105% of the mean diameter, and so on. In this way, the change in modeled pulse energy is only a result of the change in diameter because the depth was kept constant for all experiments.

Figure 9 highlights two points, the validity of the model outputs and the effect of the pulse energy on the crater diameter. To check the validity of the proposed model, the neural network outputs were compared with the available experimental data by superimposing both of them on the same graph. Figure 9 demonstrates that the ANN model outputs were consistent with experimental results. Since each point on any curve given in Fig. 9 represents crater dimensions at a particular energy level, the effect of the pulse energy on the crater diameter can be investigated as follows. Consider the

crater with 20 μm diameter and 18.1 μm depth. According to the curve labeled "*mean depth-mean diameter*", the corresponding modeled pulse energy is $E = 246.6$ μJ. If the diameter d_c is increased by 10% (i.e. the diameter is $d_{c1} = 22$ μm) while the depth is kept constant, the energy needed to produce this crater can be read from the model output curve corresponding to 110% mean diameter and found to be $E_1 = 282$ μJ. In this way, the model results presented in Fig. 9 give the relationship between the pulse energy and the crater diameter. Although E_1 and E_2 correspond to 110% and 90% mean diameter respectively, one can observe the nonlinear relationship by comparing the unequal energy difference $(E_1 - E)$ with $(E - E_2)$. However, it is worthwhile mentioning that the same technique may be used to investigate the effect of the energy on depth.

Since the curves which model the pulse energy corresponding to 80% and 50% of mean diameter lay outside the experimental data region, it is difficult to prove the validity of the model outputs for these curves. To enhance the interpretation of the available experimental data and to check the validity of the model outputs for such curves, a visualization technique is proposed. The experimental data and the model outputs can be presented graphically in 3D as shown in Fig. 10. When the pulse energy is plotted along the x-axis, the depth along the y-axis and the diameter along the z-axis, the data are found to randomly spread in planes parallel to the diameter-depth plane (i.e. y-z plane). The region within each plane where the data are spread out is confined by an elliptical boundary. The axes of the ellipse is determined using $6\sigma_{\text{depth}}$ and $6\sigma_{\text{diameter}}$, where σ_{depth} and σ_{diameter} are the standard deviations for the depths and diameters.

To interpolate values between the experimentally acquired data points, a 3D modeling software package (3D Studio MAX) was used to form a mesh that represents the volume of solutions as are illustrated in Fig. 11. In other words, points inside the mesh represent craters dimensions (depths, diameters) that correspond to specific pulse energies. When superimposing the model results of Case 3 on Fig. 11, all output curves of the ANN model fall inside the experimental data mesh except those corresponding to 80% and 50% mean diameter.

Since it is difficult to check the validity of such curves because of the lack of experimental data, the following technique was used. In Fig. 11, the model-output curves which fall inside the mesh (i.e. those which are validated by available experimental data) were connected by curve "A" at points (craters) which all have the same depth of 19.85 μm. The curve was then extended in the direction of the model-output curve corresponding to an 80% mean diameter. This extension should intersect the later curve at the point that has the same depth of all other craters on curve "A", i.e. 19.85 μm. The end point of the extension did not perfectly intersect the model-output curve at the exact point. Based on the model results, the energy at the anticipated point of intersection that corresponds to 19.85 μm was expected to be 241 μJ, while the energy at the extension endpoint was found to be 236 μJ, yielding an error of 2%. This shows that the model results are consistent for curves inside and outside the experimental data region. For verification purposes, the same technique was used with other crater depths and similar results to curve "A" were obtained.

3.2 Tests using several materials

The capability of the ANN to distinguish the energy required to create a crater of specific geometry on a particular material, when a material parameter is given as a network input, is described in this section. Once

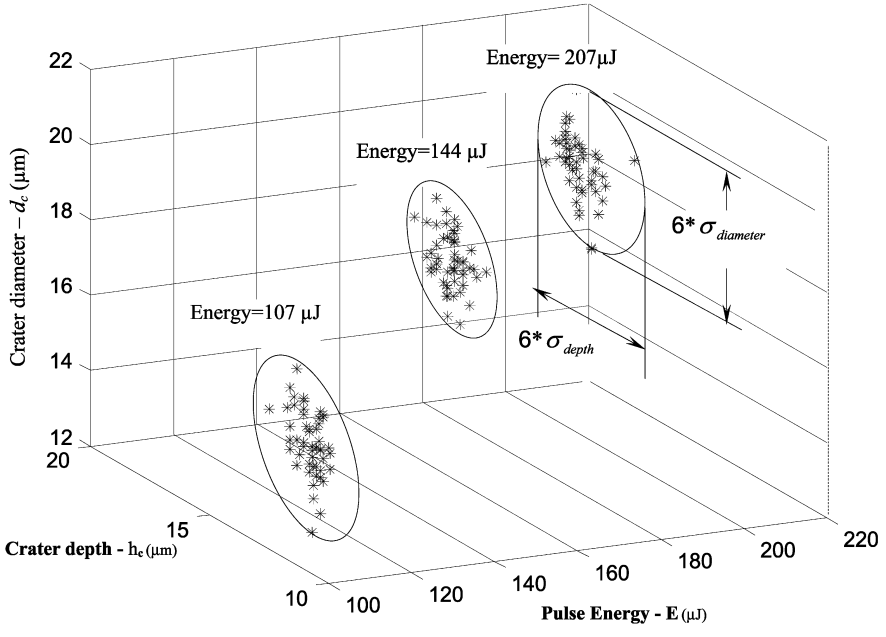

Fig. 10 Elliptical regions confining the experimental data associated with three energy levels

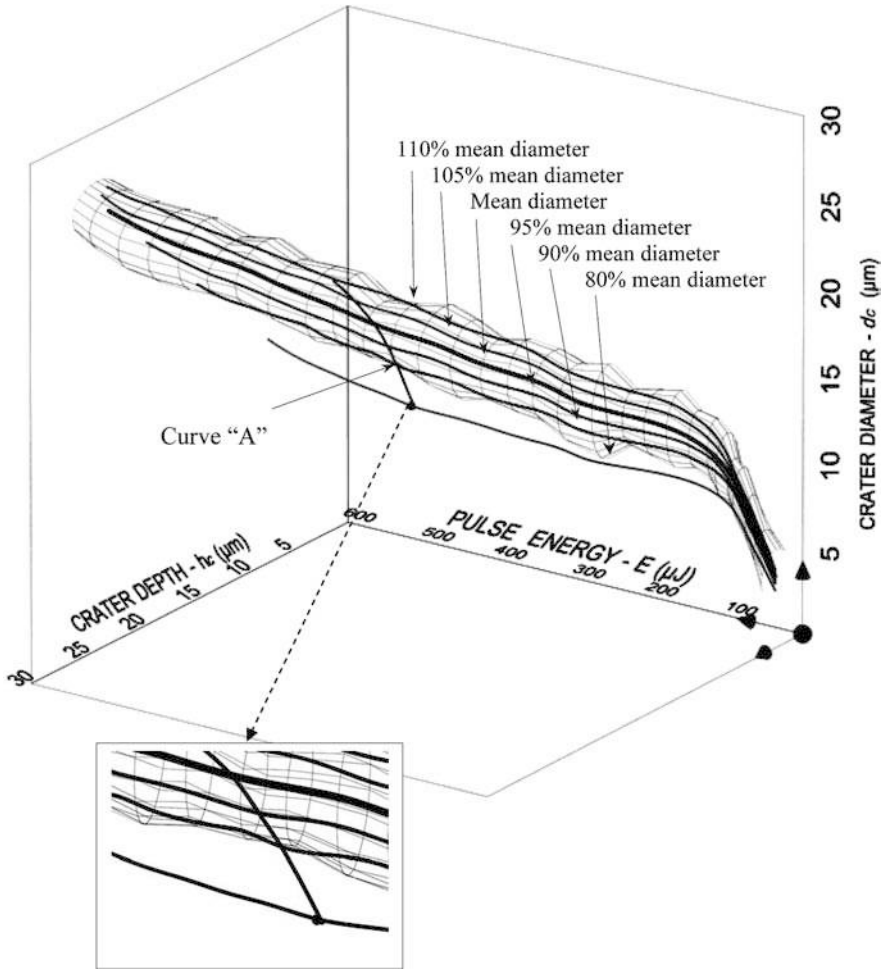

Fig. 11 All of the ANN model output curves are inside the mesh except the 80% mean-diameter curve. Curve "A" corresponds to craters having depth = 19.84 μm

again, the energy required to produce a pulse of certain geometry is modeled; but in this case, the pulses were made on different materials. Therefore, one of the inputs fed to the ANN control box is the material property. The control box for this ANN model was given in Fig. 6 where k is unique for each examined material. Before proceeding with the model results of the multi-material case, the material property selection is discussed.

The material property should be a factor that strongly affects the laser-material interaction. In other words, it must have a direct influence on the material volume melted or vaporized by a laser pulse with a given power or energy. The equation presented gives a rough estimation for the volume of material melted by a laser pulse [19]. Although it does not account for any losses and hence is very approximate, it allows one to estimate whether a given application has a chance of success or not. The equation considers the case in which laser energy E is delivered to a surface having reflectivity R, so that only the fraction (1-R) of the energy is absorbed. The beam is focused to an elliptical spot of axes a and b at the surface. Thus the volume V (or depth h_f) that can be melted by a pulse with energy E is given by

$$[c_p(T_f - T_0) + L_f]\rho V = (1 - R)E \tag{4}$$

where $V = \frac{\pi}{2}abh_f$, T_f = melting point, T_0 = ambient temperature, L_f = latent heat of fusion, and ρ = density.

From Eq. 4, it is possible to obtain some of the materials' properties that have a strong effect on the laser material removal rate. For our test purposes, the heat required to melt the volume V of a material was selected to represent the material parameter and was fed to the network as an input parameter. This is given by

$$\text{Heat of melting} = \rho c_p(T_f - T_0) \tag{5}$$

3.3 Discussion

Tests were performed using ANN1 and ANN2 to predict the pulse energy required to produce a crater with specific geometry when different materials are involved. The experimental data for brass, stainless steel and copper were fed to the ANN control box. The model outputs for the 10×5 ANN1 are shown in Fig. 12.

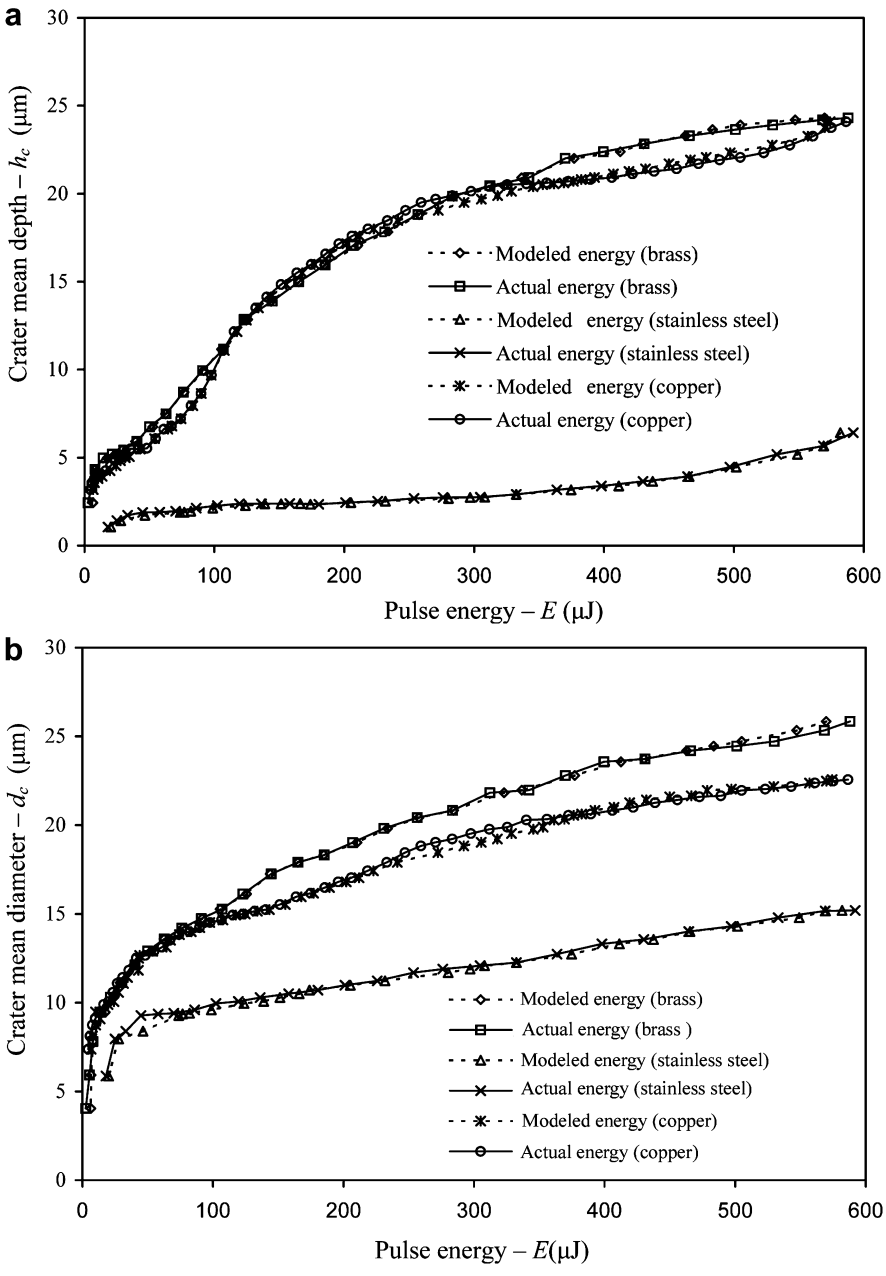

Fig. 12a–b The crater dimensions for various materials: brass, stainless steel, and copper. **a** Mean-depth of crater for experimental and ANN predicted pulse energies. **b** Mean-diameter of crater for experimental and ANN predicted pulse energies

Figure 12 shows that when the material parameter is introduced as an input, ANN1 is able to efficiently distinguish the crater geometry (i.e. mean depth and mean diameter) corresponding to a specific pulse energy for that particular material. Although the curves corresponding to brass and copper are overlapping for energies from 0 to 340 μJ, the network was successful in distinguishing the materials.

Furthermore, when the standard deviations (uncertainty measures) σ_{depth} and σ_{diameter} associated with pulse energies were modeled, ANN2 showed the same efficiency as when a single material was involved. But in this case, since the number of inputs and training patterns are larger than that of the single-material case, the number of hidden neurons was increased to (60×60) in order to achieve the desired output.

4 Conclusions

An artificial neural network approach was used to model and analyze the material removal process during laser machining. The model was developed to predict the laser pulse energy required to produce a crater with specific geometric parameters, e.g. depth and diameter, on the surface of a material foil. The model was also successful in predicting the associated variations in depth and diameter with respect to pulse energy. Experiments were carried out to provide the neural network with the necessary data for the training phase during which the network learned the process behaviour. Tests involving a single material (brass) and three materials (brass, copper and stainless steel) were used to examine the neural

network's capability of prediction. The test results showed that the ANN modeled energy corresponding to specific depth and diameter was consistent with the actual energy to a high degree of accuracy for cases when a single material and three materials were involved. In addition, the variations in depth and diameter produced by the specific energy were modeled successfully. In considering the range of capability and limitations, the model is effective in predicting the process outputs only for the specific materials which were used to train the network on the process behaviour. Furthermore, the model can be used to generate outputs for inputs that are within the range of the original input data used during the training phase.

Since the experimental conditions are likely to change due to deterioration from age and use, the adaptive properties of the network were found to be beneficial for this study. Moreover, an important benefit is that the same neural network model could easily be used many times to perform nonlinear input/output mapping without the need to amend the model. In essence, the results from the application of this model could be successfully used to study a variety of materials controlling the laser machining process parameters in order to improve the geometric quality of machined parts.

Furthermore, since the study investigated the effect of laser energy on the crater geometry, recommendations for future work include modeling the individual effect of different input parameters such as the focal spot size and frequency on the process outputs, and then extending the experimental tests to include the combined effect of those parameters on the process behaviour. This may lead to improving the process performance which eventually leads to enhancing the final product quality.

Acknowledgments The authors would also like to acknowledge the support of the National Research Council of Canada's Integrated Manufacturing Technologies Institute, and the Natural Sciences and Engineering Research Council of Canada.

Neural network training algorithm

The feedforward and back-propagation stages are shown in the following algorithm.

Step 0. Set the learning rate parameter α to 0.1 and the momentum constant μ to small values from 0.1 to 0.5. Determine the number of hidden layers as well as the number of neurons per layer. Determine the maximum number of iterations. Set the minimum system error E_{av}.

Step 1. Initialize the weights w_{ji}^{l} and biases w_{jo}^{l} for all layers to small random values between -0.1 and $+0.1$.

Step 2. While the stopping conditions are false, do Steps 3–10.

Step 3. For each training pair (X(n), $d(n)$) do Steps 4–10, where X(n) is the input signal vector at iteration n and $d(n)$ is the desired response vector at iteration n.

Step 4. Determine the response vector $\mathrm{Y}^{1}(n)$ for all the neurons in the first layer using

$$u_j^1(n) = \mathbf{W}^1(n)^{\mathrm{T}}\mathbf{X}(n) \tag{6}$$

$$y_j^1(n) = f\left(u_j^1(n)\right) \tag{7}$$

where $\mathbf{W}^1(n)$ is the interconnection weight vector for the first hidden layer neurons and f is the activation function as given by Eq. 2 which is used by the neurons of the first layer.

Step 5. Determine the response of the neurons in each of the following hidden layers as well as the output layer using

$$u_j^l(n) = \mathbf{W}^l(n)^{\mathrm{T}}\mathbf{Y}^{l-1}(n) \tag{8}$$

$$y_j^l(n) = f(u_j^l(n)) \tag{9}$$

where f is the activation function in layer l and $\mathbf{Y}^{l-1}(n)$ are the responses of neurons of the preceding layer l.

Step 6. Determine the mean squared error (or system error) $E(n)$ associated with each pattern n using

$$E(n) = \frac{1}{2}\sum_j (d_j(n) - y_j^o(n))^2 \tag{10}$$

where summation is done for all the neurons in the output layer l.

Step 7. Determine the average (normalized) system error E_{av} using

$$E_{av} = \frac{1}{N}\sum_{n=1}^{N} E(n) \tag{11}$$

where N is the total number of training patterns.

Step 8. Compute the error information terms $\delta_j^o(n)$ and calculate the weight correction terms, $\Delta w_{ji}^o(n)$, for all neurons included in the output layer o using

$$\delta_j^o(n) = (d_j(n) - y_j^o(n))f' u_j^o(n) \tag{12}$$

$$\Delta w_{ji}^o(n) = \mu\Delta w_{ji}^o(n-1) + \alpha\delta_j^o(n)y_i^l(n) \tag{13}$$

$$\Delta w_{j0}^o(n) = \mu\Delta w_{jo}^o(n-1) + \alpha\delta_j^o(n) \tag{14}$$

where the layer l is the layer preceding the output layer o.

Step 9. Compute the error information terms and the weight correction terms for all neurons in the previous (hidden) layers starting with layer l that precedes the output layer and propagate backwards up to the first hidden layer with

$$\delta_j^l(n) = \left(\sum_{k=1}^{m}\delta_k^{l+1}(n)w_{kj}^{l+1}(n)\right)f'(u_j^l(n)) \tag{15}$$

$$\Delta w_{ji}^l(n) = \mu\Delta w_{ji}^l(n-1) + \alpha\delta_j^l(n)y_i^{l-1}(n) \tag{16}$$

$$\Delta w_{jo}^l(n) = \mu\Delta w_{jo}^l(n-1) + \alpha\delta_j^l(n) \tag{17}$$

where m is the number of neurons in layer $l+1$, index k refers to neurons in the layer following layer l

and index i refers to neurons in the layer preceding layer l.

Step 10. Update weights for all layers using:

$$w_{ji}^{l}(n)_{(\text{new})} = w_{ji}^{l}(n)_{(\text{old})} + \Delta w_{ji}^{l}(n) \tag{18}$$

Step 11. Test for stopping condition

If the chosen maximum number of iterations is reached or if the normalized system error calculated in Step 7 is smaller than the pre-set value in Step 0, then STOP, otherwise continue.

References

1. Bordatchev EV, Nikumb SK (1999) Laser material-removal as a subject of automatic control. In: Proceedings of the ASPE 14th Annual Meeting, Monterey, California, USA, 236–239
2. Gonsalves JN, Duley WW (1972) Cutting thin metal sheets with the cw CO_2 Laser. J Appl Phys 43(11):4684–4687
3. Schuocker D (1987) The physical mechanism and theory of laser cutting. In: Belforte D, Morris L (eds) Annual Review of Laser Processing. Industrial Laser Handbook. Pennwell Books, pp 65–79
4. Duley WW (1976) CO_2 lasers effects and applications. Academic Press, New York
5. Kaplan AAH (1996) An analytical model of metal cutting with a laser beam. J Appl Phys 79(5):2198–2208
6. Sharkey SJ, Steen WM, Brookfield DJ (1990) Mathematical modeling of continuous wave carbon dioxide laser processing of materials using non-dimensional plots. In: ICALEO Proceedings, pp 441–450
7. Vicanek M, Simon G (1987) Momentum and heat transfer of an inert gas jet to the melt in laser cutting. J Appl Phys D 20:1191–1196
8. Schuocker D (1986) Dynamic model of laser cutting including pulsed operation. SPIE Manuf Appl Laser 621:23–30
9. Schulz W, Simon G, Urbassek HM, Decker I (1987) On laser fusion cutting of metals. J Appl Phys D 20:481–488
10. Ivarson A, Powell J, Magnusson C (1992) Laser cutting of steels: analysis of the particles ejected during cutting. Welding World 30(5,6):116–125
11. Yoshiaki A, Hiroshi M, Isamo M, Sadao T (1979) Dynamic behavior in laser gas cutting. Trans JWRI (Welding Research Institute of Osaka University, Japan) 8(2):15–26
12. Yoshiaki A, Hiroshi M, Isamo M, Sadao T (1981) Quality in laser-gas-cutting and its improvement. Trans JWRI (Welding Research Institute of Osaka University, Japan) 10(2):129–139
13. Kim MJ, Zhang J (2001) Finite element analysis of evaporating cutting with a moving high energy pulsed laser. Appl Math Model 21:203–220
14. Kim MJ, Chen ZH, Majumdar P (1993) Finite element modeling of the laser cutting process. J Comput Struct 49:231–241
15. Kim MJ, Majumdar P (1995) A computational model for high energy laser cutting process. Numer Heat Transfer A 27:717–733
16. Kaebernick H, Bicleanu D, Brandt M (1999) Theoretical and experimental investigation of pulsed laser cutting. Ann CIRP 48(1):163–166
17. Toth GJ, Szakacs T, Lorincz A (1993) Simulation of pulsed laser material processing controlled by an extended self-organizing Kohonen feature map. Mater Sci Eng B18(3):281–288
18. Haykin S (1999) Neural networks – a comprehensive foundation. Prentice-Hall, Upper Saddle River, NJ
19. Charschan SS (1993) Guide to laser materials processing. Laser Institute of America, CRC Press Inc, Boca Raton, USA